J Mater Sci (2018) 53:1658–1671

Ceramics

Electric field-assisted pressureless sintering of zirconia–scandia–ceria solid electrolytes

Eliana N. S. Muccillo[1], Sabrina G. M. Carvalho[1], and Reginaldo Muccillo[1,*]

[1] Center of Science and Technology of Materials, Energy and Nuclear Research Institute, Travessa R 400, Cidade Universitária, S. Paulo, SP 05508-170, Brazil

Received: 14 March 2017
Accepted: 19 September 2017
Published online: 22 September 2017

ABSTRACT

Electric field-assisted (flash) pressureless sintering experiments were carried out in ZrO_2 ceramics doped with 10 mol% Sc_2O_3 and 1 mol% CeO_2 (10Sc1CeSZ). All experiments were conducted isothermally at 1050 °C for 2–5 min with the application of a 100–150 V cm^{-1} AC electric field at 1 kHz with 1–4 A limiting current in green compacts and in samples pre-sintered at different temperatures. Shrinkage level, structural phases and grain morphology data were collected by dilatometry, X-ray diffraction and scanning electron microscopy analyses, respectively. The results showed that for the same delivered electric power, the final shrinkage was higher for higher temperature applications of the electric field and for higher electric current pulses. Moreover, the higher the porosity, the higher the final densification of the flash-sintered 10Sc1CeSZ samples, showing that pores play a role as a preferential path in the flash sintering mechanism.

Introduction

Oxide ion conducting solid electrolytes has applications mainly in solid oxide fuel cells, chemical species sensors and ceramic membranes for gas separation [1, 2]. Zirconia–yttria solid solutions (ZrO_2: x mol% Y_2O_3, $x = 3$ and 8) are the most studied O^{2-} conducting polycrystalline ceramics due to their relatively large oxide ion conductivity (0.1 S cm^{-1} at 1000 °C for $x = 8$, suitable for Solid Oxide Fuel Cells, SOFCs) [3], chemical inertness across a wide temperature range, and commercial availability [4]. Research has been conducted over a long period to look for oxide ion conductors with an ionic conductivity of the same order of magnitude of that of zirconia: 8 mol% yttria (8YSZ), but at lower temperatures [2, 5, 6]. This would provide a way for designing SOFCs operating at temperatures lower than 1000 °C, avoiding many technical problems that occur at high temperatures, for example, the disruption of these devices due to a mismatch of the coefficients of thermal expansion of the SOFC components (electrolyte, anode and cathode) [7]. The substitution of scandia for yttria in zirconia solid electrolytes was proposed due to the improvement in ionic conductivity; however, zirconia–scandia ceramics have a temperature-dependent multi-phase constitution inhibiting their use; furthermore, SOFC

Address correspondence to E-mail: muccillo@usp.br

DOI 10.1007/s10853-017-1615-3

thermal cycling promotes phase change with volume variation leading to disruption of the cell [8]. Doping with another metal oxide (aside from scandium oxide) was proposed as a solution, and cerium oxide has been considered the most successful for the full stabilization of the cubic phase at room temperature [9, 10]. 10Sc1CeSZ conventionally sintered at 1150–1300 °C presents a mixture of cubic and rhombohedric phases [11], and spark plasma sintered at 1200 °C destabilizes the cubic zirconia [12] due to the Ce^{4+}–Ce^{3+} reduction. This means that sintering 10Sc1CeSZ requires special attention to the experimental conditions to preserve the cubic structure [13–15]. A single SOFC is composed of a dense solid electrolyte and porous ceramic anode and cathode. Usually the anode–electrolyte–cathode setup is sintered simultaneously (co-firing) as the solid electrolyte requires relatively high temperatures to achieve full density, and the anode and cathode require lower temperatures to become porous to allow for gas evolution through their structure.

Electric field-assisted pressureless sintering is a technique that has been largely applied in the last decade to YSZ [16–25] and is known as flash sintering when the event has a primary heating source of direct Joule heating occurring in short times (0.1–60 s) [26, 27]. This technique consists of applying a DC or AC electric field to a polycrystalline ceramic at temperatures lower than conventional temperatures for sintering, thus promoting densification in relatively short times, usually without considerable grain growth [26, 28].

In this study, the results on electric field-assisted pressureless sintering (hereafter "flash sintering") of 10 mol% scandia − 1 mol% ceria–zirconia solid electrolytes are reported for the first time. The microstructure and the electrical conductivity of flash-sintered specimens were also studied. The aim was to show the difference in the electrical behavior of flash-sintered specimens under different experimental conditions (temperature, delivered electric power and porosity).

Materials and methods

$(Sc_2O_3)_{0.10}(CeO_2)_{0.01}(ZrO_2)_{0.89}$ (10Sc1CeSZ) commercial ceramic powders of 10–12 $m^2\ g^{-1}$ surface area were used [29]. The powders were uniaxially pressed in ϕ 5–14 mm and thickness 2–5 mm cylindrical shape at 10 MPa and isostatically at 200 MPa. The geometrical density was ~ 45% TD (TD: theoretical density = 5.90 g cm^{-3} [29]).

X-ray diffraction analyses were carried out at the flat surfaces of the as-sintered 10Sc1CeSZ pellets in a D8 Advance Bruker-AXS diffractometer in Bragg–Brentano configuration with Cu-k_α radiation, scintillation detector, in the 20°–80° 2θ range, 0.02° step size, 10 s per step. EVA® software was used for background subtraction and peak search.

For the flash sintering experiments, 10Sc1CeSZ green or pre-sintered cylindrical pellets (after being covered with a diluted platinum paste for the uniformity of the electric current pulse) were positioned into the sample holder of a Unitherm 1161 Anter vertical dilatometer and platinum grids placed on both parallel surfaces of the sample were connected with platinum wires to a homemade power supply operating at 5–65 V/0.5–6.0 A in the 0.5–1.1 kHz frequency range. The applied voltage and the electric current data through the specimen were collected in two Fluke 8050A multimeters and stored in a computer. Figure 1 shows the typical data applying 150 V cm^{-1}, limiting the current to 4 A.

The experimental procedure used for flash sintering experiments was first described in detail elsewhere [19]. In short, it consists of collecting dilatometric data (linear shrinkage × sample temperature) while heating the sample to a chosen temperature below the conventional sintering temperature, applying an electric field up to the occurrence of an electric current surge where the electric field may be applied once or as many times as required for reaching a desired shrinkage level that

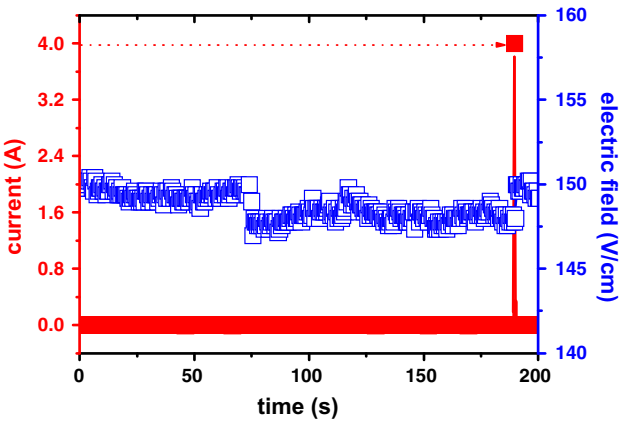

Figure 1 Profiles of electric current and electric field during application of 150 V cm^{-1} to 10Sc1CeSZ limiting the current to 4 A.

was monitored in the dilatometer gauge. During the occurrence of the electric current pulse, the temperature achieved by the specimen depends on the amount of Joule heating produced through the specimen which, in turn, depends on the amplitude of the electric field, the number of current pulses and the preset electric current limit. This work was based on previous experiments on flash sintering in stabilized zirconia solid electrolytes [16, 18–25], and the applied electric field was 100–150 V cm^{-1} at 1 kHz and the limit current 1–4 A. Aside from the experiments with the green compacts, pellets previously heated at different temperatures were also flash sintered to verify the effect of the electric current pulse in samples with different pore volumes. Some samples were sintered at 1400 °C for comparison with flash sintered samples. The apparent density of the sintered specimens was determined by the Archimedes method with a Mettler AG245 analytical balance with distilled water as the liquid medium.

Impedance spectroscopy measurements were carried out with a 4192A Hewlett Packard LF impedance analyzer connected to a series 360 Hewlett Packard Controller. Three specimens, with silver paste covering the parallel surfaces and cured at 400 °C, were positioned inside an Inconel 600 sample chamber, which was inserted in a programmable furnace. The measurements were performed in the $f = 5$ Hz to 13 MHz frequency range at 400–545 °C in the oxide ion conductivity region of the stabilized zirconias. Special software was used to control the impedance analyzer and for the collection and deconvolution of the $[-Z''(\omega) \times Z'(\omega)]$ impedance data, Z'' and Z' are the imaginary and the real component of the impedance, respectively, and $\omega = 2\pi f$ [30].

The external surfaces of the conventional and flash-sintered samples were observed in an Inspect F50 FEI field emission gun scanning electron microscope. The surfaces were first abraded with silicon carbide powders, followed by polishing with diamond pastes (15–1 μm), thermally etched at 1350 °C/15 min and sputtered with gold.

Results

Conventional sintering

Figure 2a shows the dilatometric curve of 10Sc1CeSZ heated up to 1400 °C and down to 400 °C at 10 °C

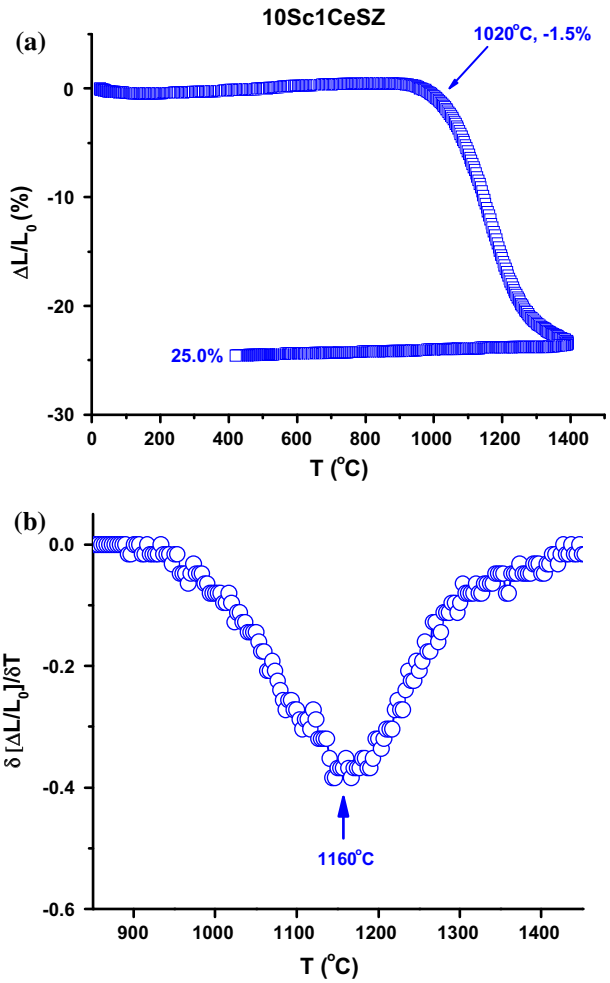

Figure 2 **a** Dilatometric curve of 10Sc1CeSZ in the room temperature −1400 to 400 °C range; heating and cooling rates were 10 °C min^{-1}; and **b** the first derivative of the dilatometric curve with inflection point 1160 °C.

min^{-1} heating and cooling rates. The ϕ 5 mm × 3 mm green pellet reached 25.0% longitudinal shrinkage. The density evaluated by the Archimedes method was 5.60 g cm^{-3} (∼ 95% TD). The derivative minimum of the dilatometric curve (Fig. 2b) for evaluation of the temperature of the maximum shrinkage rate was 1160 °C. There was no shrinkage up to the onset of the second stage of sintering at approximately 900 °C. The temperature of 1020 °C was chosen to apply the electric field as at that temperature, the specimen is in the intermediate stage of sintering and the pore phase is still continuous [31], thus being a percolation path for easy flow of charge carriers.

Flash sintering at different temperatures

Figure 3 shows the dilatometric curves of specimens with application of the electric field for 5 min at three temperatures: 960, 1020 and 1200 °C. These results provide evidence of the dependence of the final shrinkage attained by a 10Sc1CeSZ green pellet on the temperature to which an electric field is applied. As the temperature increases, the mobility of charge carriers increases according to its dependence on the Boltzmann factor. The increase in mobility may facilitate the electric current flow through the specimen, promoting higher delivery of Joule heating, with a consequent increase in densification.

The scanning electron microscopy micrographs of the specimen sintered at 1400 °C to near full density (Fig. 2a) and flash sintered at 960, 1020 and 1200 °C (Fig. 3) are shown in Fig. 4. The micrographs on the left side of the figure were taken at the flat polished and thermally etched surfaces of the cylindrical samples; and the micrographs on the right side were taken in the inner part (bulk) of the samples after sawing them normal to their thickness, polishing and thermally etching.

The distribution of grain sizes of the specimens shown in Fig. 4 is displayed in the histograms presented in Fig. 5a–h. The conventionally sintered 10Sc1CeSZ showed larger grains at the bulk than at the external surface. All 10Sc1CeSZ flash-sintered specimens presented a larger content of smaller

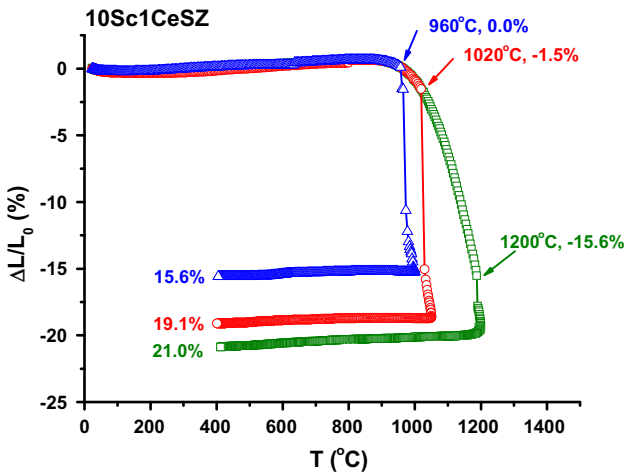

Figure 3 Dilatometric curves of 10Sc1CeSZ flash sintered at 960, 1020 and 1200 for 5 min with 100 V cm^{-1}, 1 kHz, 1 A limit current.

grains when compared to the conventionally sintered specimen. In particular, the 10Sc1CeSZ specimen flash sintered at 960 °C presented larger amounts of relatively smaller grains. Another feature was that the distributions of grain sizes of flash-sintered specimens were somewhat sharper than that of the conventionally sintered specimen.

Impedance spectroscopy measurements were carried out in both the conventionally and flash-sintered samples (Figs. 2a, 3). The data collected at 450 °C were plotted as $[-Z''(f) \times Z'(f)]$ impedance diagrams in Fig. 6. That temperature was selected as it is within the electrolytic window of 10Sc1CeSZ with predominant oxide ion conductivity [10–15] allowing for discrimination of the bulk and grain boundary contributions to electrical resistivity [32, 33]. The impedance diagram of the conventionally sintered sample at 1400 °C was composed of two semicircles with their centers located below the Z' axis, one at high frequencies due to the intragranular (bulk) contribution to the resistivity, and the other at lower frequencies due to the intergranular (interfaces) contribution.

The thermally activated process of electrical resistivity was ascertained by impedance spectroscopy measurements at several temperatures for the specimens flash sintered at 1020 °C. The impedance data collected at 480, 495 and 545 °C with the corresponding $[Z''(\omega) \times \log f]$ Bode diagrams are shown in Fig. 7a. Bode diagrams are useful for better visualizing the frequency dependence of the impedance [32, 33]. Figure 7c shows the temperature dependence of the total resistivity (measured at the intercept with the real axis at the low frequency end of the impedance diagram).

Flash sintering with different delivered electric power

Figure 8 shows the dilatometric curves of 10Sc1CeSZ with the application of 150 V cm^{-1} at 1020 °C for 5 min, limiting the maximum electric current to 1, 2 and 4 A. All samples had the same dimensions and weight, with a green density of ~45%. The shrinkages for limiting the current to 1, 2 and 4 A were 7.8, 22.7 and 29.6%, respectively. The latter was larger than the value achieved with the 1400 °C conventional sintering (Fig. 2a).

Figure 9 shows scanning electron microscopy micrographs of the flat surfaces of the specimens

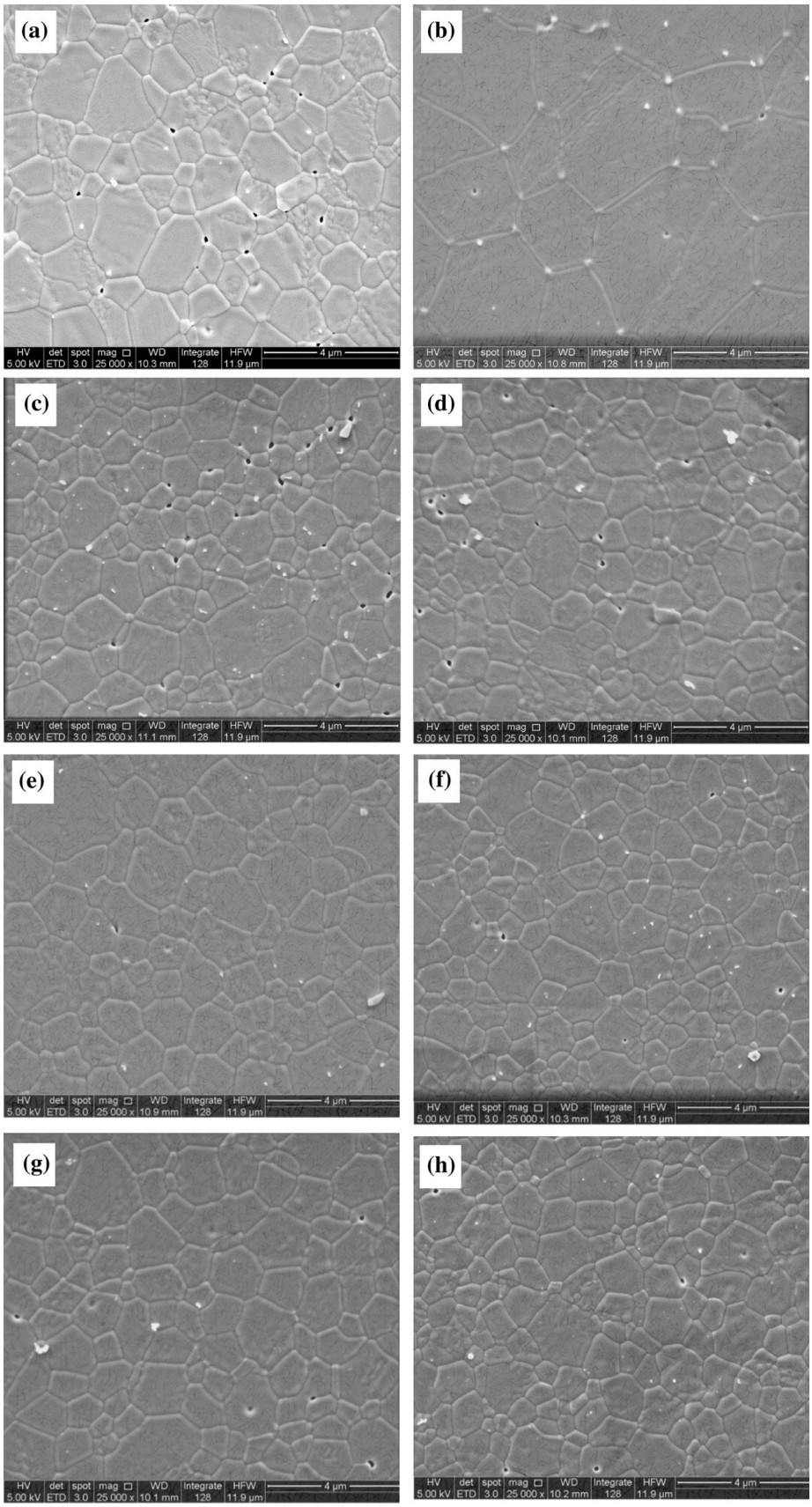

Figure 4 Scanning electron microscopy micrographs (surface-left, bulk-right) of 10Sc1CeSZ conventionally sintered at 1400 °C (**a**, **b**) and flash sintered at 960 °C (**c, d**), 1020 °C (**e**, **f**) and 1200 °C (**g**, **h**) for 5 min with 100 V cm^{-1}, 1 kHz, 1 A limiting current.

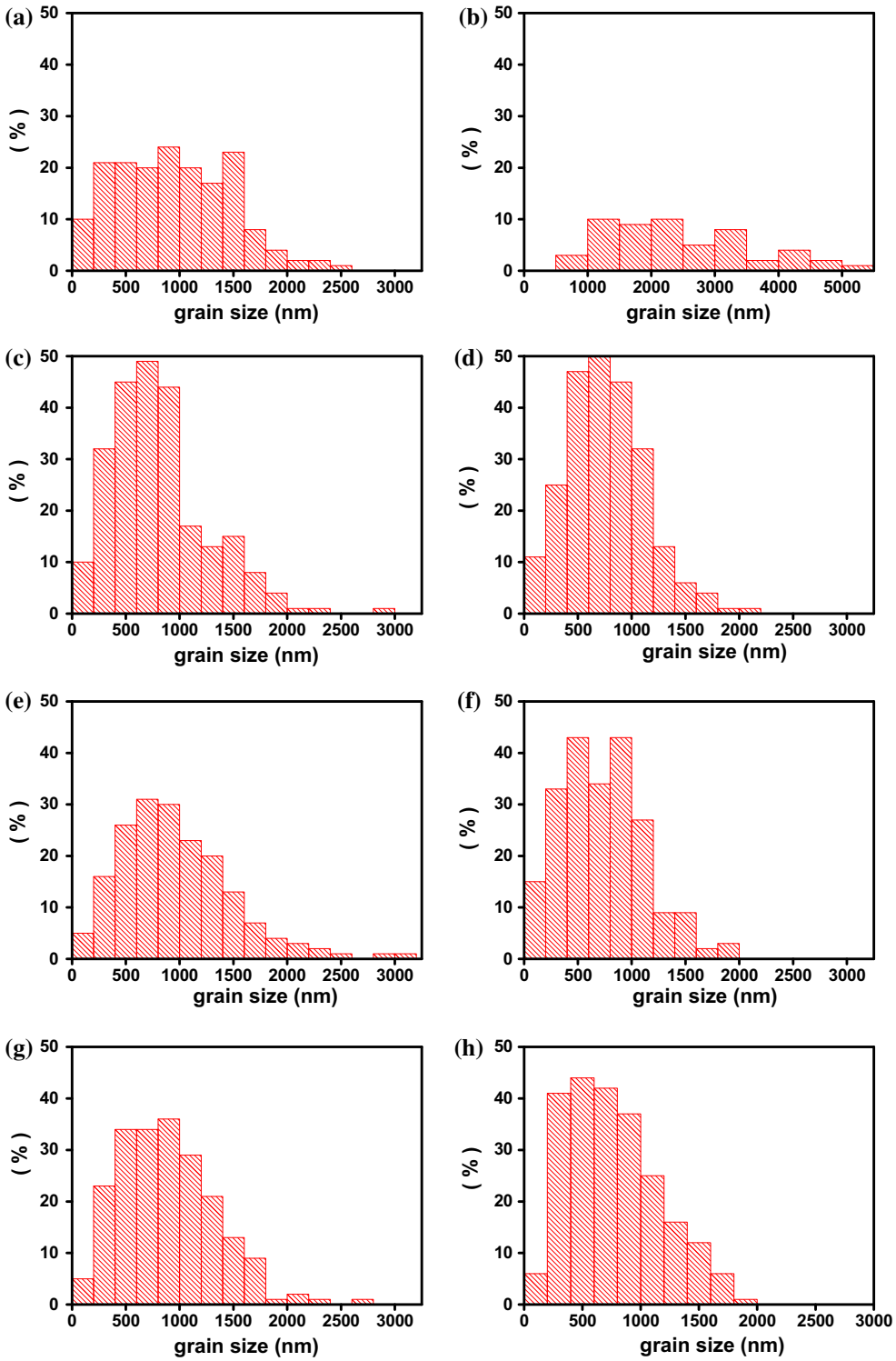

Figure 5 Histograms of grain sizes of 10Sc1CeSZ conventionally sintered at 1400 °C (**a**, **b**) and flash sintered at 960 °C (**c, d**), 1020 °C (**e**, **f**) and 1200 °C (**g**, **h**). (SEM micrographs in Fig. 4).

flash sintered at 1020 °C with 150 V cm^{-1}, 1 kHz, limiting the current to (a) 1 A, (b) 2 A and (c) 4 A (Fig. 8) and (d) sintered at 1400 °C (Fig. 2a).

The impedance spectroscopy diagrams of the 10Sc1CeSZ samples flash sintered at 1020 °C, with 1, 2 and 4 A limiting current amplitudes are

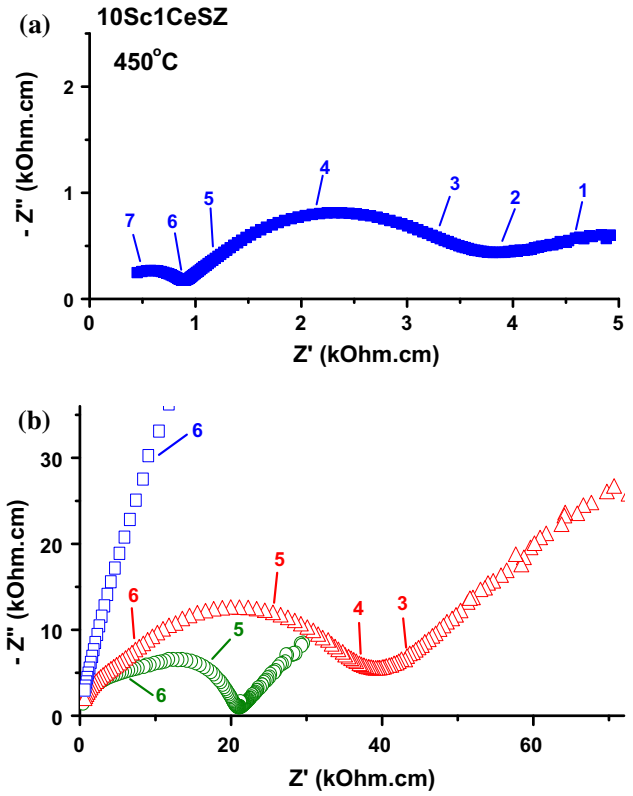

Figure 6 Impedance spectroscopy plots of 10Sc1CeSZ. (**a**) After conventional sintering at 1400 °C; and (**b**) flash sintered at 960 °C—square, 1020 °C—triangle and 1200 °C—circle for 5 min with 100 V cm^{-1}, 1 kHz, 1 A limiting current. Temperature of measurement: 450 °C. Numbers stand for log*f* (Hz).

shown in Fig. 10a (measured at 400 °C), 10b (450 °C).

Flash sintering samples with different porosities

Many experiments on flash sintering have been reported on several electroceramics with the application of an electric field at different temperatures [26, 28]. Care has not been taken when describing the actual microstructure of the specimens before, but only after sintering. The distribution of the electric field throughout the specimen may be dependent on the available pathways for the electric current pulse as well as on the available charge carriers; therefore, their character and concentration are dependent on the temperature. Mechanisms based on partial softening/melting at the interfaces due to thermal runaway caused by Joule heating [34, 35] and the high diffusivity of defects at the molten interfaces (again, caused by Joule heating [36, 37]) were proposed. In

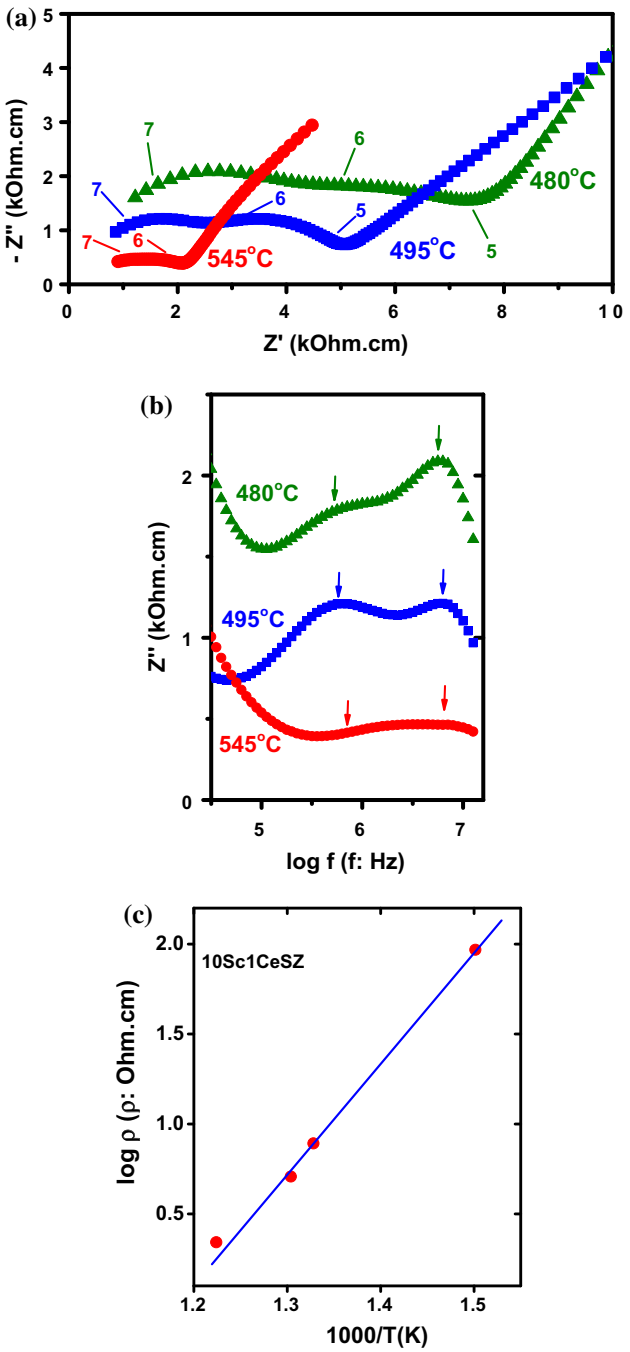

Figure 7 Impedance spectroscopy plots of 10Sc1CeSZ. **a** Flash sintered at 1020 °C for 5 min with 100 V cm^{-1}, 1 kHz, 1 A limiting current. Temperatures of measurement: 480, 495 and 545 °C; numbers stand for log*f* (Hz); **b** Bode diagrams of the reactance evaluated from the impedance diagrams in (**a**), the arrows pointing to the frequency maximum; and **c** Arrhenius plot of the total resistivity.

this paper, we report a simple series of experiments that considered that pores were connected and pore volume decreased with increasing temperatures in

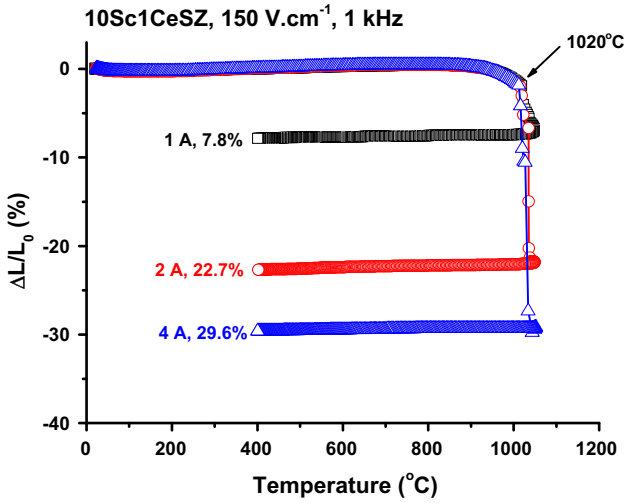

Figure 8 Dilatometric curves of 10Sc1CeSZ with application for 5 min at 1020 °C of 150 V cm^{-1}, 1 kHz, limiting the current to 1 A—square, 2 A—circle and 4 A—triangle; heating and cooling rates: 10 °C min^{-1}.

the second stage of sintering (900–1400 °C, Fig. 2), so specimens with different pore volumes were prepared. Three similar samples were heated up to 900 °C (at the first sintering stage with the promotion of neck growth among particles [31, 38]), 1000 and 1300 °C, (both at the second sintering stage already had interconnected pores [31, 38]) and cooled down to room temperature inside the dilatometer, recording their shrinkage. Afterward, each sample was heated to the same temperature, 1020 °C, and a 100 V cm^{-1} electric field was applied for 5 min. The dilatometric results are shown in Fig. 11. Apparently, the higher the available pore volume (lower pre-sintering temperature), the higher is the shrinkage level (900 °C = 17.0%, 1000 °C = 7.5% and 1300 °C = 4.1%).

Figure 12 shows the scanning electron microscopy micrographs of the surfaces of 10Sc1CeSZ ceramic pellets after the flash sintering experiments depicted in Fig. 11.

Figure 13 shows the impedance spectroscopy diagrams measured at 450 °C in 10Sc1CeSZ ceramics exposed at 1020 °C for 5 min to 100 V cm^{-1}, 1 kHz, 1 A limiting current; (a), (b) and (c) refer to specimens pre-sintered at 900, 1000 and 1300 °C, respectively.

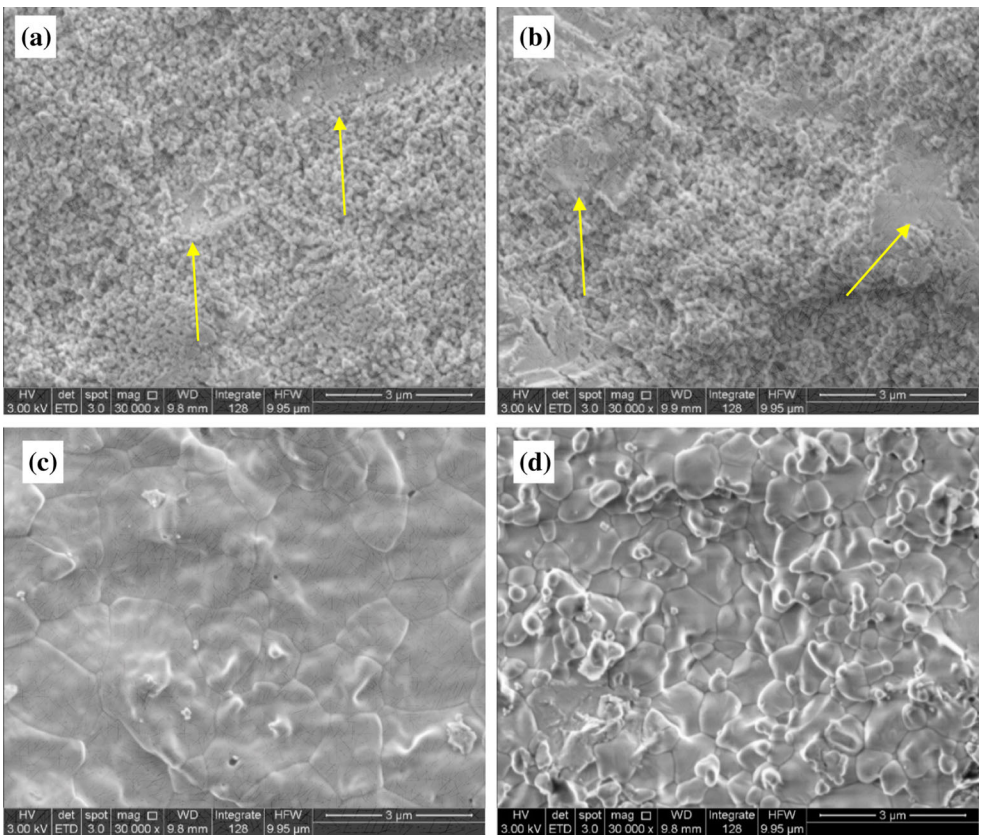

Figure 9 Scanning electron microscopy micrographs of 10Sc1CeSZ flash sintered at 1020 °C for 5 min with 150 V cm^{-1}, 1 kHz with 1 A (**a**); 2 A (**b**); 4 A (**c**); and sintered at 1400 °C (**d**).

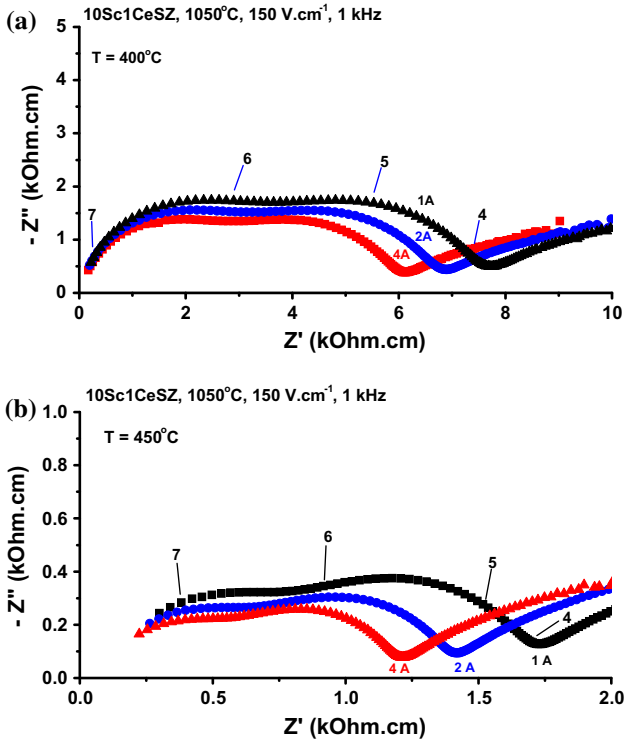

Figure 10 Impedance spectroscopy plots of 10Sc1CeSZ after flash sintering at 1050 °C for 5 min with 150 V cm^{-1}, 1 kHz, limiting the current to **a** 1 A—square; **b** 2 A—circle; and **c** 4 A—triangle. Temperatures of measurement are 400 °C (**a**) and 450 °C (**b**). Numbers stand for log*f* (Hz).

X-ray diffraction of conventional and flash-sintered samples

Figure 14 shows the results of X-ray diffraction analysis performed at room temperature for two 10Sc1CeSZ sintered samples: one heated at 10 °C min^{-1} up to 1400 °C for 2 h and cooled down to room temperature at the same rate; and another heated at 10 °C min^{-1} to 1000 °C, kept at that temperature for 5 min under 100 V cm^{-1} limiting to 1 A the current through the sample and cooled down to room temperature at the same rate. Both samples presented a single fluorite cubic phase.

Discussion

Conventional and flash sintering at different temperatures

Sintering the 10Sc1CeSZ green compact at 1400 °C produced a ceramic pellet with 95% relative density with a 25% linear shrinkage (Fig. 2a). The X-ray

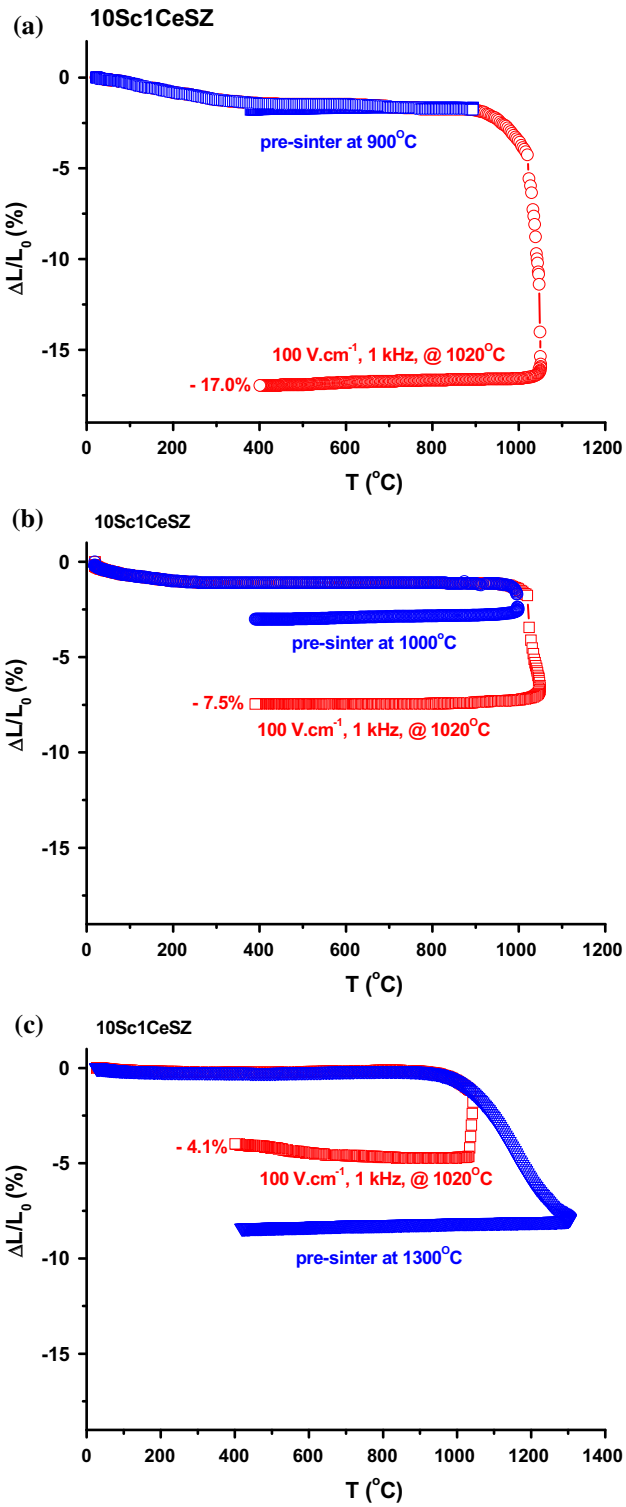

Figure 11 Dilatometric curves of 10Sc1CeSZ flash sintered at 1020 °C for 5 min with 100 V cm^{-1}, 1 kHz, 1 A limiting current. Specimens were pre-sintered at **a** 900 °C, **b** 1000 °C and **c** 1300 °C.

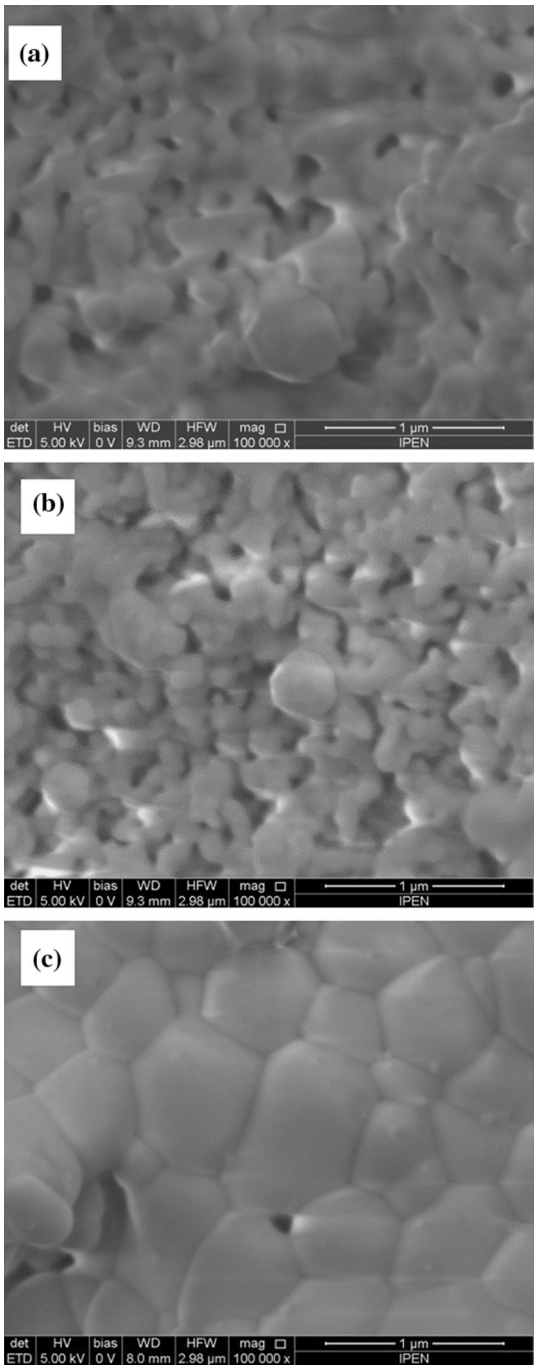

Figure 12 Scanning electron microscopy micrographs of 10Sc1CeSZ flash sintered at 1020 °C with 100 V cm^{-1}, 1 kHz, 1 A limiting current. Specimens pre-sintered at **a** 900 °C; **b** 1000 °C; and **c** 1300 °C.

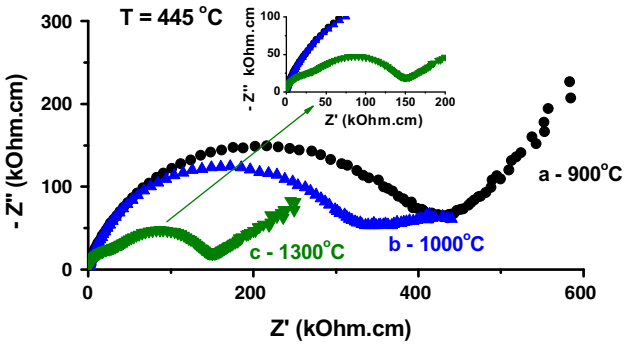

Figure 13 Impedance spectroscopy plots of 10Sc1CeSZ pre-sintered at **a** 900 °C—circle; **b** 1000 °C—triangle; and **c** 1300 °C—square, flash sintered at 1050 °C for 5 min with 100 V cm^{-1}, 1 kHz, 1 A limiting current. Temperature of measurement: 450 °C. Numbers stand for log*f* (Hz). Inset: zoom of impedance plots of specimens pre-sintered at 1000 °C—triangle and 1300 °C—square.

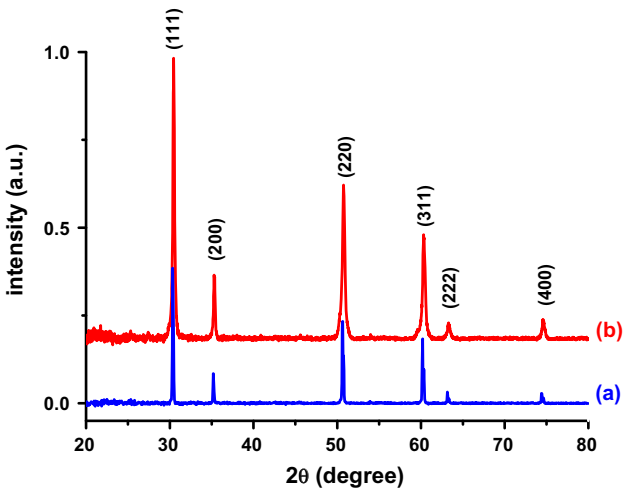

Figure 14 X-ray diffraction patterns of 10Sc1CeSZ. *a* Sintered at 1400 °C; and *b* flash sintered at 1000 °C; numbers refer to Miller indexes of the cubic phase.

diffraction analysis of the pellet surface only showed reflections of the cubic fluorite phase (Fig. 14) [10–15].

The application of an electric field in a 10Sc1CeSZ compact at temperatures below 1400 °C made the compact shrink, and the shrinkage level dependent on the temperature the field was applied. In Fig. 3, for same applied electric field (100 V cm^{-1}) and limiting current (1 A), the achieved shrinkage levels at 960, 1020 and 1200 °C were 15.6, 19.1 and 21.0% and the maximum shrinkage rate temperatures were 970, 1026 and 1189 °C (evaluated at the inflection points of the derivatives of the dilatometric curves), respectively. It should be noted that the experiments were reproducible: In the conventional sintering, when the sample reached 1020 °C, the shrinkage was 1.5% (Fig. 2), and the same value was measured when a similar sample was heated to 1020 °C for the application of the electric field (Fig. 3). The primary

effect of increasing the temperature from 960 to 1020 °C, and further to 1200 °C was a decrease in the electrical resistivity, and consequently, an increase in the charge carriers' mobility, thus enhancing grain boundary diffusivity, which is reported as the main mechanism for sintering zirconia [39, 40], and densification. It is worth noting that the difference in shrinkage (60 °C in the sample temperature) was from about 15.6–19.1%, whereas a further increase of 180–1200 °C resulted in an additional 1.9% increase in the shrinkage (from about 19.1 to 21.0%). It is well known that sintering ceramic bodies usually follows three well-defined stages: the initial stage with the accommodation of particles and interparticle neck growth; the intermediate stage with equilibrium of pore shapes and continuous pores; and the final stage usually with pore elimination and grain growth [31, 38]. These results showed that the linear shrinkage produced by the application of the electric field was higher for higher pore fraction in the solid electrolyte. The small difference in shrinkage level (1.9% when applying the electric field at 1020 and 1200 °C) was because, in the latter, the majority of the pores were already eliminated [31, 38].

The scanning electron microscopy micrographs of the samples conventionally sintered at 1400 °C and flash sintered at three different temperatures showed that the sample sintered at 1400 °C was dense as expected, and the average grain size was in the micrometer range (Fig. 4a), and the bulk (Fig. 4b) had slightly larger average grain sizes. The SEM micrographs of the flash-sintered samples, on the other hand, (Fig. 4c–h), showed similar average grain sizes at surface and bulk, which might have been a consequence of the large temperature achieved due to intergranular Joule heating [26, 41, 42], and residual intergranular pores. A careful inspection of several micro-regions in all samples in the micrographs collected under the same conditions showed that the main difference between conventionally sintered and flash-sintered samples was that in the latter, the grains at the surface and at the bulk had approximately the same average grain size while in the former, the grains differed in size from the surface to the bulk. The histograms in Fig. 5 show the distribution of grain sizes.

The samples resulting from the dilatometric behavior shown in Figs. 2 and 3 had their densities evaluated: 5.60 g cm^{-3} (94.9% T.D., conventional sintering, Fig. 2), 3.70 g cm^{-3} (62.7%), 4.13 (70.0%) and 5.20 g cm^{-3} (88.1%) (flash-sintered samples, Fig. 3). The increase in the shrinkage was due to a reduction in the thickness and diameter of the flash-sintered sample, which resulted from a collapse of the grains because of the neck formation promoted by Joule heating [18].

The total resistivity was approximately 4 kΩ cm at 450 °C for the conventionally sintered sample (Fig. 6a). After extrapolation to the different temperatures reported, this value was of the same order of magnitude of values published by other authors [11–13, 43, 44]. The depression in the high-frequency semicircle was due to the distribution of grain sizes, as seen in Figs. 4a, b and 5a, b; in the low frequency semicircle, the reason may be the intergranular pores, as seen in Fig. 4a, b. The $[-Z''(f) \times Z'(f)]$ impedance diagram of the flash-sintered sample at 960 °C (Fig. 6b) had apparently only one semicircle—meaning one response in frequency—due to the large density of the intergranular area, including porosity. The impedance diagram of the sample flash sintered at 1200 °C, on the other hand, was composed of two well-defined semicircles, as evidenced by the intragranular (bulk) and the intergranular (grain boundaries) contributions to resistivity, and a spike at the very low frequencies was due to electrode (Pt + Ag) polarization [32, 33]. The impedance diagram of the sample flash sintered at 1020 °C (still in the first stage of sintering, Fig. 2) also showed two semicircles, i.e., the separation in two electrical responses, due to grains and interfaces. A large difference in the total resistivity was determined: 4 and 20 kΩ cm for the conventional and the sample flash sintered at 1200 °C, respectively. The impedance diagram (consisting of two semicircles, with one in the high-frequency region (HF: 10^6–10^7 Hz) and the other in the low frequency region (LF: 10^6–10^4 Hz) was deconvoluted in frequency, providing the following associated electrical resistivity ρ: $\rho_{HF} = 1$ kΩ cm and $\rho_{LF} = 3$ kΩ cm for the conventionally sintered sample; $\rho_{HF} = 8$ kΩ cm and $\rho_{LF} = 12$ kΩ cm for the flash sintered sample.

Impedance spectroscopy data were also collected at different temperatures: 395, 480, 495 and 545 °C. Some of the $[-Z''(\omega) \times Z'(\omega)]$ and $[Z''(\omega) \times \log f]$, impedance (Fig. 7a) and Bode (Fig. 7b) diagrams, respectively, plotted in Fig 7, shows the two components due to the lattice and the grain boundaries responses. Figure 7c, the plot of the total electrical resistivity as a function of the reciprocal temperature,

shows the expected Arrhenius behavior, allowing for the evaluation of the activation energy $E = 1.16$ eV, based on the Arrhenius equation $\rho = \rho_0 \times \exp(E/kT)$. This value was in agreement with the reported values 1.15 ± 0.05 [12] and 1.18 ± 0.03 eV [45].

Flash sintering with different delivered electric power

The electric power delivered to a specimen in the flash sintering experiments is the product of the electric field to the electric current. The power supply used was designed to set a limit to the maximum electric current through the specimen, keeping the electric voltage constant. In Fig. 8, three experimental data are reported for 150, 300 and 600 W electric power. To increased electric power, there was an increase in the shrinkage level. Higher electric power was avoided due to possible thermal runaway with damage to the dilatometer sample holder. The explanation for the achieved shrinkage levels was that increased electric power through the sample produced increased Joule heating, which led to an even larger local temperature. This increase in temperature at the intergranular region may have been responsible for mass diffusivity from grain to grain, leading to densification [18, 26, 27].

For the 1 and 2 A limiting currents, the grains were in the submicron range, there was intergranular porosity, and apparent dense regions were seen. Even though grain growth was suppressed, the micrographs showed that there were preferential pathways for the electric current through the specimen, thereby producing denser regions. For the 4 A limiting current, a highly dense ceramic was obtained. The grains are much larger in Fig. 9c than in Fig. 9a, b, the Joule heating in this case being sufficient not only to create necks among particles, but also to promote grain growth. The grains were even larger than in the conventionally sintered sample at 1400 °C, a possible indication that the local temperature achieved values higher than 1400 °C.

There was a decrease in the total resistivity for increasing the limit current during the flash sintering according to Fig. 10, as expected due to the increased density. The diagrams were composed of two well-defined semicircles, with a spike at the low frequency range ($< 10^4$ Hz). The semicircles were due to the contributions from the bulk (higher frequencies, $f > 10^6$ Hz) and the interfaces (lower frequencies, $10^6 < f < 10^4$ Hz, grain boundaries and pores) [32, 33]. The following values were evaluated for the associated total resistivity: 7.7, 6.9 and 6.0 kΩ cm for flash-sintered samples with 1, 2 and 4 A, respectively.

Flash sintering samples with different porosities

It was apparent in Fig. 11 that 10Sc1CeSZ samples heat treated up to the first stage of sintering (900 and 1000 °C) achieved higher shrinkage levels (17 and 7.5%) than the sample heat treated up to the second stage of sintering (1300 °C, 4.1%), which indicates that pores might be pathways for the current pulse during application of the electric field. These results were in agreement with the flash sintering mechanisms proposed by Chaim [34, 35] and Narayan [36, 37] on the occurrence of Joule heating at available interfaces to promote shrinkage.

In samples pre-sintered at 900 and 1000 °C, there was a decrease in porosity, an increase in densification and a slight increase in the average grain size, all within the submicron average size range. The sample pre-sintered at 1300 °C, on the other hand, was nearly fully dense with little intergranular porosity. The results of the impedance spectroscopy measurements of these samples (carried out at 450 °C) are presented in Fig. 13.

Even though the shrinkage attained by the 10Sc1CeSZ samples was higher for the lower pre-sintering temperatures, their total electrical resistivity, as shown in Fig. 13, was higher due to the larger density of pores [46].

X-ray diffraction of conventional and flash-sintered samples

The effectiveness of flash sintering (compared to conventional sintering, which used lower temperatures and times to achieve full density) was confirmed by no difference in the composition of the structural phase. Figure 14 shows the results of the X-ray diffraction analysis of 10Sc1CeSZ pellets sintered conventionally and with an application of an electric field. The reflections of both samples were identical and belonged to the fluorite cubic phase [9–15].

Conclusions

The 10Sc1CeSZ green ceramic samples conventionally sintered at 1400 °C presented lower values of electrical resistivity than the flash sintered (at 900, 1050 and 1200 °C) samples. It was assumed that the intergranular porosity in the flash-sintered samples, as observed in the SEM micrographs, contributed to the electrical resistivity due to the interfacial blocking of oxide ions. Electric field-assisted pressureless sintering pre-sintered samples showed that the higher the average pore volume, the higher the attained shrinkage level under the same experimental conditions, meaning that pores may act as available pathways for the electric current pulse through the sample during sintering. The X-ray diffraction experiments showed that the samples sintered by applying an electric field kept a cubic fluorite structural phase.

Acknowledgements

To Comissão Nacional de Energia Nuclear—CNEN, Conselho Nacional de Desenvolvimento Científico e Tecnológico—CNPq (Procs. 470952/2013-0, 303483/2013-0) and Fundação de Amparo à Pesquisa do Estado de São Paulo—FAPESP (Proc. 2013/07296-2) for financial support. One of the authors (SGMC) acknowledges Coordenação de Aperfeiçoamento de Pessoal de Nível Superior (CAPES) for the doctorate scholarship.

Compliance with ethical standards

Conflict of interest The authors declare there is no conflict of interest.

References

[1] Hagenmuller P, Van Gool W (1978) Solid electrolytes, characterization, materials, applications. Academic Press, Cambridge

[2] Goodenough JB (2003) Oxide-ion electrolytes. Annu Rev Mater Res 33:91–128

[3] Minh NQ (1993) Ceramic fuel cells. J Am Ceram Soc 76:563–588

[4] Stevens R (1986), Magnesium Elektron Publ. N. 113

[5] Wachsman ED, Lee KT (2011) Lowering the temperature of solid oxide fuel cells. Science 334:935–939

[6] Singh B, Ghosh S, Aich S, Roy B (2017) Low temperature solid oxide electrolytes (LT-SOE): a review. J Power Sources 339:103–135

[7] Kawada T, Sakai N, Yokokawa H, Doriya M, Anzai I (1992) Relation between solid oxide fuel-cell materials. Solid State Ionics 50:189–196

[8] Mizutani Y, Tamura M, Kawai M, Yamamoto O (1994) Development of high-performance electrolyte in SOFC. Solid State Ionics 72:271–275

[9] Lee D-S, Kim WS, Choi SH, Kim J, Lee H-W, Lee J-H (2005) Characterization of ZrO_2 co-doped with Sc_2O_3 and CeO_2 electrolyte for the application of intermediate temperature SOFCs. Solid State Ionics 176:33–39

[10] Wang ZW, Cheng MJ, Bi ZH, Dong YL, Zhang HM, Zhang J, Feng ZC, Li C (2005) Structure and impedance of ZrO_2 doped with Sc_2O_3 and CeO_2. Mater Lett 59:2579–2582

[11] Grosso RL, Muccillo ENS (2013) Sintering, phase composition and ionic conductivity of zirconia-scandia-ceria. J Power Sources 233:6–13

[12] Grosso RL, Bertolete M, Machado IF, Muccillo R, Muccillo ENS (2013) Ionic conductivity and phase stability of spark plasma sintered scandia and ceria-stabilized zirconia. Solid State Ionics 230:48–51

[13] Tan J, Su Y, Tang H, Hu T, Yu Q, Tursun R, Zhang X (2016) Effect of calcined parameters on microstructure and electrical conductivity of 10Sc1CeSZ. J Alloy Compd 686:394–398

[14] Ramesh S, Ng CK, Tan CY, Wong WH, Ching CY, Muchtar A, Somalu MR, Ramesh S, Chandran H, Devaraj P (2016) Effects of sintering on the mechanical and ionic properties of ceria doped scandia stabilized zirconia ceramic. Ceram Int 42:14469–14474

[15] Tan J, Su Y, Hu T, Yu Q, Tursun R, Li Q, Yunze X (2016) Preparation and conductivity of Sc_2O_3–CeO_2–ZrO_2. Solid State Ionics 292:22–26

[16] Cologna M, Prette ALG, Raj R (2011) Flash-sintering of cubic yttria-stabilized zirconia at 750 °C for possible use in SOFC manufacturing. J Am Ceram Soc 94:316–319

[17] Muccillo R, de Florio DZ, Fonseca FC, Muccillo ENS (2014) Electric field-assisted co-sintering of planar anode-supported solid oxide fuel cell. MRS fall meeting 2014

[18] Muccillo R, Kleitz M, Muccillo ENS (2011) Flash grain welding in yttria stabilized zirconia. J Eur Ceram Soc 31:1517–1521

[19] Muccillo R, Muccillo ENS (2013) An experimental setup for shrinkage evaluation during electric field-assisted flash sintering: application to yttria-stabilized zirconia. J Eur Ceram Soc 33:515–520

[20] Downs JA, Sglavo VM (2013) Electric field assisted sintering of cubic zirconia at 390 degrees C. J Am Ceram Soc 96:1342–1344

[21] Steil MC, Marinha D, Aman Y, Gomes JRC, Kleitz M (2013) From conventional ac flash sintering of YSZ to hyper-flash and double flash. J Eur Ceram Soc 33:2093–2101

[22] Muccillo R, Muccillo ENS (2014) Shrinkage control of yttria-stabilized zirconia during ac electric field-assisted sintering. J Eur Ceram Soc 34:3871–3877

[23] Muccillo R, Muccillo ENS (2014) Light emission during electric field-assisted sintering of electroceramics. J Eur Ceram Soc 35:1653–1656

[24] da Silva JGP, Lebrun J-M, Al-Qureshi HA, Janssen R, Raj R (2015) Temperature distributions during flash sintering of 8% yttria-stabilized zirconia. J Am Ceram Soc 98:3525–3528

[25] Du YX, Stevenson AJ, Vernat D, Diaz M, Marinha D (2016) Estimating Joule heating and ionic conductivity during flash sintering of 8YSZ. J Eur Ceram Soc 36:749–759

[26] Yu M, Grasso S, McKinnon R, Saunders T, Reece MJ (2016) Review of flash sintering: materials, mechanisms and modelling. Adv Appl Ceram 116:24–60

[27] Muccillo R, Muccillo ENS (2016) Electric field assisted sintering of electroceramics and in situ analysis by impedance spectroscopy. J Electroceramics 38:24–42

[28] Dancer CEJ (2016) Flash sintering of ceramic materials. Mater Res Express 3:1–25

[29] https://fuelcellmaterials.com/products/powders/electrolyte-powders/scandia-ceria-stabilized-zirconia-10-sc-1-ce-powder/

[30] Kleitz M, Kennedy JH (1979) Resolution of multicomponent impedance diagrams. In: Mundy JN, Shenoy GK, Vashishta P (eds) Fast ion transport in solids. Elsevier, North Holland, pp 185–188

[31] Rahaman MN (2008) Sintering of ceramics. CRC Press, Boca Raton, p 56

[32] Macdonald JR (1987) Impedance spectroscopy, emphasizing solid materials and systems. Wiley, London

[33] Déportes C, Duclot M, Fabry P, Fouletier J, Hammou A, Kleitz M, Siebert E, Souquet JL (2008) Électrochimie des Solides. Grenoble Sciences, Grenoble

[34] Chaim R (2016) Liquid film capillary mechanism for densification of ceramic powders during flash sintering. Materials 9:1–8

[35] Chaim R (2017) Particle surface softening as universal behaviour during flash sintering of oxide nano-powders. Materials 10:1–9

[36] Narayan J (2013) Grain growth model for electric field-assisted processing and flash sintering of materials. Scr Mater 68:785–788

[37] Narayan J (2013) A new mechanism for field-assisted processing and flash sintering of materials. Scr Mater 69:107–111

[38] German RM (1996) Sintering theory and practice. Wiley, London

[39] Boutz MMR, Winnubst AJA, Burgraaff AJ (1994) Yttria-ceria stabilized tetragonal zirconia polycrystals: sintering, grain-growth and grain boundary segregation. J Eur Ceram Soc 13:89–102

[40] Matsui K, Yamakawa T, Uehara M, Enomoto N, Hojo J (2008) Sintering mechanism of fine zirconia powders with alumina added by powder mixing and chemical processes. J Mater Sci 43:2745–2753. doi:10.1007/s10853-008-2493-5

[41] Jha SK, Terauds K, Lebrun J-M, Raj R (2016) Beyond flash sintering in 3 mol% yttria stabilized zirconia. J Ceram Soc Jpn 124:283–288

[42] Dong Y, Chen I-W (2016) Thermal runaway in mold-assisted flash sintering. J Am Ceram Soc 99:2889–2894

[43] Badwal SPS, Drennan J (1992) Microstructure conductivity relationship in the scandia zirconia system. Solid State Ionics 53:769–776

[44] Badwal SPS, Ciacchi FT, Rajendran S, Drennan J (1998) An investigation of conductivity, microstructure and stability of electrolyte compositions in the system 9 mol% (Sc_2O_3–Y_2O_3)–ZrO_2(Al_2O_3). Solid State Ionics 109:167–186

[45] Fu Y-P, Wen S-B, Lu C-H (2008) Preparation and characterization of samaria-doped ceria electrolyte materials for solid oxide fuel cells. J Am Ceram Soc 91:127–131

[46] Muccillo R (2009) Impedance spectroscopy analysis of zirconia: 8 mol% yttria solid electrolytes with graphite pore former. J Mater Res 24:1780–1784